FULL PAPER

ADVANCED
ENGINEERING
MATERIALS
www.aem-journal.com

Check for updates

Additively Manufactured Polyetheretherketone (PEEK) with Carbon Nanostructure Reinforcement for Biomedical Structural Applications

Fahad Alam, Kartik M. Varadarajan, Joseph H. Koo, Brian L. Wardle, and Shanmugam Kumar*

This study is focused on carbon nanostructures (CNS), including both carbon nanotubes (CNTs) and graphene nanoplatelets (GNPs), reinforcement of medical-grade polyetheretherketone (PEEK), and in vitro bioactivity for biomedical structural applications. CNS/PEEK scaffolds and bulk specimens, realized via fused filament fabrication (FFF) additive manufacturing, are assessed primarily in the low-strain linear-elastic regime. 3D printed PEEK nanocomposites are found to have enhanced mechanical properties in all cases while maintaining the desired degree of crystallinity in the range of 30–33%. A synergetic effect of the CNS and sulfonation toward bioactivity is observed—apatite growth in simulated body fluid increases by 57% and 77%, for CNT and GNP reinforcement, respectively, doubling the effect of sulfonation and exhibiting a fully-grown mushroom-like apatite morphology. Further, CNT- and GNP-reinforced sulfonated PEEK recovers much of the mechanical losses in modulus and strength due to sulfonation, in one case (GNP reinforcement) increasing the yield and ultimate strengths beyond the (non-sulfonated) printed PEEK. Additive manufacturing of PEEK with CNS reinforcement demonstrated here opens up many design opportunities for structural and biomedical applications, including personalized bioactivated surfaces for bone scaffolds, with further potential arising from the electrically conductive nanoengineered PEEK material toward smart and multifunctional structures.

1. Introduction

Polyetheretherketone (PEEK) is a semi-crystalline high-temperature structural polymer, originally developed by Imperial Chemical Industries, UK, in 1977.[1] It has excellent mechanical and fatigue properties, and chemical resistance,[2] making it suitable for many demanding structural applications, such as aerospace structures. In addition, PEEK is bioinert with excellent biocompatibility and has recently been investigated for its potential use in load-bearing orthopedic and dental applications.[3] Ultrahigh-molecular-weight polyethylene and metals have been the "gold standard" in these biomedical application areas, but high-performance polymers such as PEEK are increasingly being considered in the orthopedic community to replace one or both. PEEK is a promising alternative to metal alloys to address issues of metallic corrosion, bone-implant stiffness mismatch, and radiopacity. PEEK is a particularly attractive material choice for orthopedic subspecialties, such as total joint replacements and trauma. PEEK is processed by a variety of synthesis routes, including compression

Dr. F. Alam, Prof. S. Kumar
Department of Mechanical Engineering
Khalifa University of Science and Technology
Masdar Campus, Masdar City, P.O. Box 54224, Abu Dhabi, UAE
E-mail: s.kumar@eng.oxon.org

Dr. K. M. Varadarajan
Department of Orthopaedic Surgery
Harris Orthopedics Laboratory
Massachusetts General Hospital
55 Fruit St, Boston, MA 02114, USA

Dr. K. M. Varadarajan
Department of Orthopaedic Surgery
Harvard Medical School
A-111, 25 Shattuck Street, Boston, MA 02115, USA

Dr. J. H. Koo
Department of Mechanical Engineering
The University of Texas at Austin
Austin, TX 78712, USA

Prof. B. L. Wardle
Department of Aeronautics and Astronautics
Massachusetts Institute of Technology
Cambridge, MA 02139, USA

Prof. S. Kumar
James Watt School of Engineering
University of Glasgow
Glasgow G12 8LT, UK

The ORCID identification number(s) for the author(s) of this article can be found under https://doi.org/10.1002/adem.202000483.

molding, extrusion, and injection molding.[4] These techniques have the limitation of processing implants optimally customized to the patient's anatomy[5] and often introduce geometric mismatch with native bone once implanted in the patient. With the help of additive manufacturing (AM) (aka 3D printing), a patient's specific implant can be more effectively addressed and implant designs better matched to native physiology can be realized.[6] Thus, PEEK in AM (selective laser sintering (SLS)[7,8] and fused filament fabrication (FFF, aka fused deposition modeling, FDM)[9]) can create improved implant structures tailored to individual application sites, and here we report[10] on carbon nanostructure (CNS)-reinforced PEEK for FFF[9] AM as a cost-effective alternative to SLS.

In FFF AM, a polymer filament is fed through a preheated nozzle to enable a layer-by-layer deposition to build a 3D structure. This involves motion of the print head in the X- and Y- axes, while lowering the print bed in the Z-axis.[7] After each layer of deposition, the print bed is lowered and another layer is deposited on top of the preceding layer in a pattern dictated by the desired computer-aided design (CAD) model.[8] FFF is the most widely used AM technique due to its ease of use, fast fabrication, cost effectiveness, and ability to produce complex geometries without involving postmachining.[11] A variety of polymers and their composites can be processed by FFF, such as acrylonitrile butadiene styrene,[12] polylactic acid,[13] polyamides,[14] polypropylene,[15] and polycarbonate.[16,17] AM of high-temperature structural (modulus in excess of 1 GPa) thermoplastics, such as PEEK, has received enormous attention because of their wide applicability in many areas, including aerospace, energy, and orthopedics.[18]

As with many other thermoplastic materials, PEEK's mechanical properties can be further improved with nanoreinforcements, such as carbon nanomaterials.[18a] The ability to spatially tailor the elastic modulus of PEEK to closely match properties of native bone is indispensable for avoiding problems, such as stress shielding. Furthermore, there is currently a lack of diagnostic methods to measure device performance in situ (once it is implanted in, or affixed to, the patient). The hybridization of PEEK via the addition of electrically conductive micro/nanofillers can introduce piezoresistivity, which can be utilized for sensing device performance.[10a,c,19] In this study, we developed CNS-reinforced PEEK filament feedstocks for FFF AM, and we demonstrate the ability to print bioactive scaffolds utilizing medical-grade CNS-reinforced PEEK nanocomposites. CNS reinforcement includes carbon nanotubes (CNTs) and graphene nanoplatelets (GNPs). In vitro bioactivity and mechanical characteristics of 3D printed scaffolds and mechanical test specimens are analyzed considering biomedical scaffold applications, for example, scaffolds to assist in tissue support and repair after severe trauma. The focus is on the behavior in the nonhysteretic low-strain linear-elastic regime for these biomedical structural applications. The bioactivity tests reveal a synergy between the CNS and the effectiveness of the chemical treatment (sulfonation) used to enhance bioactivity on the PEEK surface.[20]

2. Experimental Section

2.1. Materials

Filaments of PEEK (Victrex PEEK 450G, by Apium Additive Technologies GmbH) and nanocarbon-reinforced PEEK (PEEK/CNT and PEEK/GNP filaments developed by the authors utilizing melt extrusion at KAI, LLC, Austin, Texas, USA) all having diameter of 1.75 mm were used for the fabrication of all test specimens (for microstructural analysis of filament feedstocks, please refer to Figure S1, Supporting Information). It is important to note that all commercial PEEK grades and types are not the same and their properties such as the degree of crystallinity and molecular structure will manifest in various ways, affecting the thermal, physical, and mechanical characteristics, depending upon the inherent properties of the PEEK grade chosen and synthesis route adopted.[21] The PEEK/CNT filament contains 1 wt% of CNT, while the PEEK/GNP contains 3 wt% of GNP. These CNS loadings were found to be processible into uniform filaments in preliminary work. The concentration of CNS is chosen such that they form electrical percolation in the 3D printed PEEK but still remain biocompatible.[22] Three samples each of PEEK, PEEK/CNT, and PEEK/GNP without and with sulfonation (indicated with prefix "S", e.g., S-PEEK/CNT) for bioactivation (see Section 2.3) were prepared for testing. Sulfuric acid used for sulfonation of samples was purchased from Merck chemicals and utilized without dilution (95–97%). Simulated body fluid (SBF) was prepared in the laboratory using analytical grade salts, following the method proposed by Kokubo and colleagues.[23]

2.2. FFF 3D Printing

All specimens were fabricated using FFF (Indmatec HPP 155 FFF 3D printer, Apium Additive Technologies GmbH) AM. The feeding of the filaments into a nozzle of 0.4 mm diameter was enabled by pressure feed mechanism via a driver motor and a counter-rotating set of grooved gears. To determine the slicing sequence and other printing parameters, Simplify3D software (Simplify3D, Cincinnati, Ohio) was utilized. The printing parameters for specimen fabrication are listed in **Table 1**. For better adhesion, the nozzle movement speed and temperature of the first layer were set to be different from the rest of the layers. A glue (water-soluble, DimaFix, print bed glue) was manually applied on the surface of the glass bed to adhere the first layer of the fabricated specimen. A brim was added, which helps in holding the edges of the fabricated specimen, and selected process parameters were adopted from our previous study on 3D-printed neat PEEK.[18a] Note that process parameters were kept the same for all cases. An overview and representative

Table 1. Printing parameters for preparing all specimens.

Parameters	Parameters used
Speed of nozzle movement	1000 mm min^{-1}; first layer: 300 mm min^{-1}
Nozzle temperature	410 °C; first layer: 390 °C
Bed temperature	100 °C
Layer height	0.1 mm; first layer: 0.18 mm
Extrusion width	0.48 mm
Infill pattern	Rectilinear (raster angle 0°)
Infill density	60% (40% porous) for bioactivity scaffold specimens, and 100% (0% porosity) for tensile specimens

**ADVANCED
SCIENCE NEWS**
www.advancedsciencenews.com

**ADVANCED
ENGINEERING
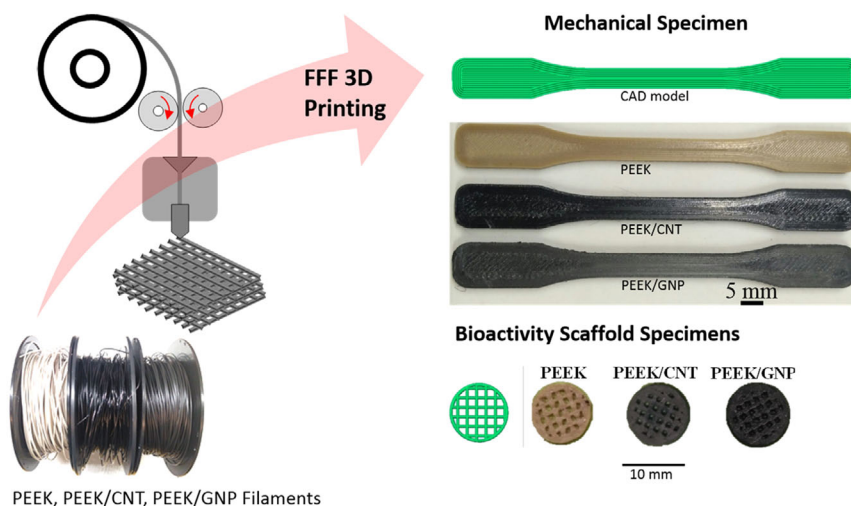MATERIALS**
www.aem-journal.com

Figure 1. Nanoengineered PEEK filaments are used to 3D print (via FFF) mechanical dogbone and bioactivity scaffold specimens. CAD model of specimen is shown in green.

images of 3D printed samples for bioactivity and mechanical tests are shown in **Figure 1**. The internal morphology of fractured surfaces and the layered architecture of 3D printed samples are shown in Figure S2, Supporting Information.

2.3. Bioactivation of 3D Printed Samples

PEEK is known to have relatively low osteoconductive properties relative to other implant materials, such as stainless steel and titanium. Therefore, it is desirable to enhance the osteoconductive behavior of implant surfaces made of PEEK that interface with native bone.[24] There are a number of approaches that have

been adopted to improve the bioactivity of PEEK, such as changing surface roughness, using bioactive fillers, and chemical modification.[25] Sulfonation is one of the chemical approaches for changing surface property where sulfuric acid is used to modify the surface morphology of PEEK through etching action. Sulfonation of PEEK has mostly been exploited for ion-exchange membranes[26] used in fuel cell applications,[27] although a few recent studies have emerged on biomedical applications of sulfonated PEEK.[3a,18e,28] The sulfonation of mechanical dogbone and cylindrical bioactivity scaffold samples were performed by dipping them into concentrated (12 mol) sulfuric acid (H_2SO_4) for 5 min (selected from literature) at room temperature followed by thorough (3×) rinsing with deionized (DI) water (see **Figure 2**).
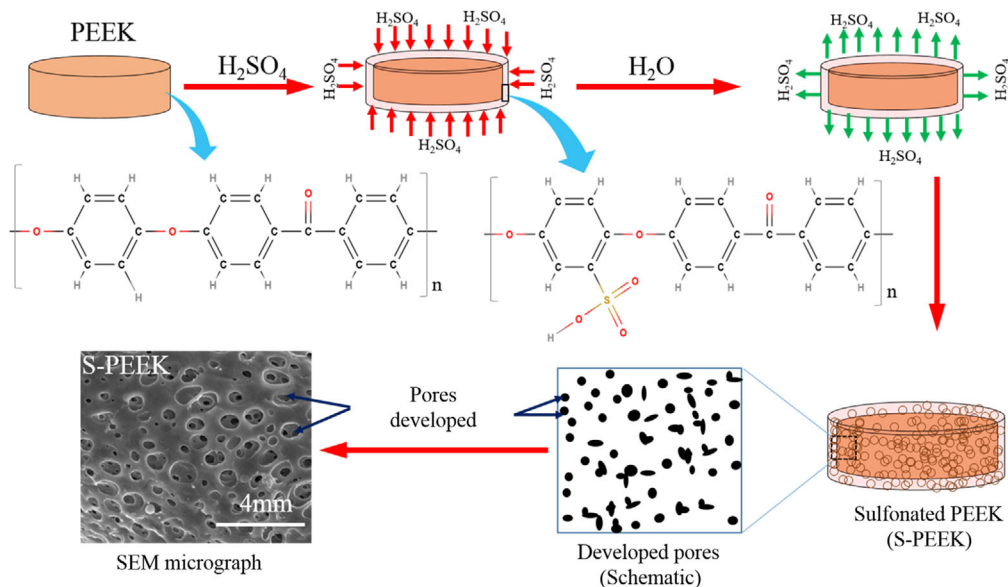

Figure 2. Schematic diagram of sulfonation process of PEEK and its nanocomposite samples processed by FFF 3D printing. The steps involved in the sulfonation are shown, where samples are exposed to sulfuric acid followed by rinsing with water. The developed pores are shown in the schematic in the white box with black dots. The SEM image shows the porous structure of PEEK after sulfonation.

ADVANCED
SCIENCE NEWS
www.advancedsciencenews.com

ADVANCED
ENGINEERING
MATERIALS
www.aem-journal.com

To produce uniform pores from the etching action, the sulfonation was done in a continuous stirring condition using a magnetic stirrer. The samples were then dried overnight in an oven at 50 °C before testing.

2.4. Thermophysical and Surface Properties of 3D-Printed PEEK Samples

It is well known that hard nanostructures, principally CNS, can have strong morphological effects on the polymer when nanocomposites are prepared, significantly altering properties of the polymer local to the CNS.[29] As a broad category, thermoplastics are known to oftentimes have enhanced crystallinity due to the incorporation of CNS; that is, the CNS act to promote crystallization. Further, PEEK is a semi-crystalline polymer with the degree of crystallinity as a critical parameter controlled via processing to achieve desired properties. Nevertheless, as indicated before, these effects depend on the PEEK grade and type.[21] Differential scanning calorimetry (DSC) was performed using a DSC 404, F1 (NETZSCH high-temperature DSC) instrument under a nitrogen flux of 20 mL min^{-1}. Three samples for each specimen type of ≈10 mg were subjected to a heating scan of 25–420 °C, at a rate of 10 °C min^{-1}, to evaluate the glass transition (T_g) and melting (T_m) temperatures, where the melting temperature and heat of fusion were taken from the second heating cycle to eliminate the influence of thermal history.[30] The degree of crystallinity (χ_c) of the samples was calculated[31] by $\chi_c = \Delta H_c \times 100/(\Delta H_c^0 w)$, where ΔH_c is the heat of crystallization and ΔH_c^0 is the heat of crystallization of 100% crystalline PEEK (130 J g^{-1}),[32] and w is the mass fraction of PEEK in the nanocomposites.

The surface topography of all the samples with and without sulfonation was observed using scanning electron microscopy (SEM, the FEI Nova NanoSEM 650) with an accelerating voltage of 15 kV and a working distance of 5 mm. A thin layer of Ag/Pt (10 nm) was deposited on the surface, by sputtering, for SEM imaging. Surface wettability plays a major role in osseointegration as hydrophilic surfaces are favorable toward basic cell interaction mechanisms such as adhesion and proliferation;[33] however, there are other factors that may affect bioactivity, such as surface roughness, surface porosity, and the presence of functional groups.[34] The surface hydrophilicity of the samples was measured using a contact angle goniometer (Krüss GmbH's Drop Shape Analyzer, DSA, Germany) by adding a 5 μL drop of DI water on the surfaces of the samples through a needle, following the Sessile drop method in static mode.[35] On each sample, at least three droplets were formed at different locations and the average of the contact angle values was reported.

2.5. Mechanical Properties of 3D-Printed PEEK Samples

Uniaxial quasi-static tensile tests were conducted on dogbone samples using a Zwick-Roell Z005 universal testing machine fitted with a 2.5 kN load cell, at a constant crosshead speed of 1 mm min^{-1} at ambient temperature (≈24 °C) as per ASTM D638 standard. For proper calculation of the elastic modulus, digital image correlation (DIC) analysis was used to assess the strain field in the gauge section. Three specimens of each sample were tested and the average values reported with standard error. Yield stress was calculated at 1% strain offset. The standard allows modulus and yield strength to be quantified, and is often used to assess ultimate strength as done here.[36] The fractured surfaces of the samples after static fracture was observed using an SEM.

2.6. In Vitro Bioactivity Testing

In vitro bioactivity tests on all samples were conducted by immersing them in the SBF, a solution with ion concentrations and a pH value similar to those of human body fluid, with supersaturated calcium and phosphate. SBF was prepared by following the method proposed by Kokubo and colleagues.[37] This method of bioactivity assessment has been widely reported in the literature as an efficient initial test for bioactivity.[38] It is predicated on the assumption that a material that can have apatite mineral formed on its surface in SBF will induce apatite formation in vivo, and hence better bonding to living bone.[39] Samples were immersed in SBF for 72 h in an incubator at 37 °C and then dried in an oven at 50 °C overnight and examined under an SEM to assess the growth of apatite on the surface of the samples. These grown apatite layers were further characterized by X-ray diffraction (XRD) to confirm and quantify the presence of the apatite layer.[40] Cu Kα radiation ($\lambda = 1.541$ Å) operated at 25 kV and 15 mA was used as X-ray source (using an XRD PANalytical Empyrean diffractometer) with a scan speed of 2.4° min^{-1} and step size of 0.02° with 2θ ranging from 10° to 60°.

3. Results and Discussion

The nanoengineered PEEK filaments developed here were utilized in the FFF AM process described in Section 2 to print mechanical test specimens and scaffolds for testing bioactivity (Figure 1). First, we discuss the physical characteristics of the nanoengineered PEEK structures achieved via FFF and then present the results of the bioactivity experiments, which reveal a synergy between the CNS reinforcement of the fibers and the sulfonation process used to increase bioactivity.

3.1. Properties of 3D Printed Nanoengineered PEEK Structures

As discussed in Section 2.2, understanding the degree of crystallinity of the printed PEEK structures is important to ascertain whether the CNS has altered this important microstructural characteristic that dictates the performance of PEEK composites. The thermographs obtained from the DSC analysis of PEEK (and sulfonated PEEK) samples are shown in **Figure 3** and the corresponding thermal properties obtained are shown in **Table 2**. It is evident from the DSC scans that CNS serve as nucleating agents permitting molecular chains of PEEK to pack into a closer arrangement.[41] Thus, the degree of crystallinity of PEEK increases by 3% and 2% with the addition of 1 wt% CNT and 3 wt% GNP, respectively. Note that the increase in degree of crystallinity is more for lower concentration of CNS, as reported elsewhere.[22] The values of degree of crystallinity after 3D printing are slightly lower than those reported for the parent PEEK. However, it should be noted that the extrusion effect is dictated by the chemistry, composition, and molecular
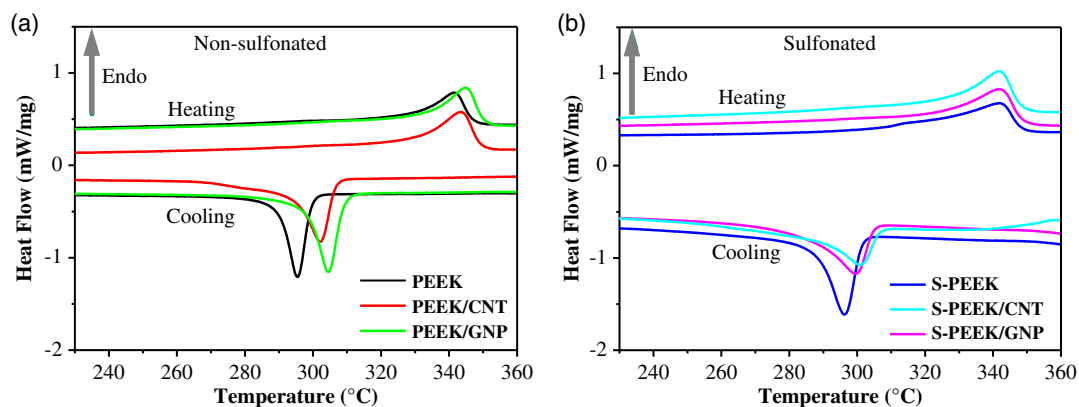
Figure 3. Representative DSC thermographs of a) PEEK and b) S-PEEK with CNS reinforcement, showing melting temperature, crystallization temperature, and heat flow for melting and crystallization. Summary data are listed in Table 2.

Table 2. Thermal properties and degree of crystallization obtained from DSC analysis.

Samples	T_m [°C]	T_c [°C]	ΔH_m [J g^{-1}]	ΔH_c [J g^{-1}]	Crystallinity [%]
PEEK	341.6 ± 0.49	297.00 ± 1.41	30.06 ± 1.21	40.06 ± 0.02	31.40 ± 0.84
S-PEEK	341.5 ± 0.21	296.50 ± 2.12	29.56 ± 1.11	39.03 ± 1.42	30.70 ± 0.98
PEEK/CNT	344.2 ± 0.28	298.95 ± 5.72	30.00 ± 1.90	42.52 ± 0.17	34.23 ± 1.74
S-PEEK/CNT	342.3 ± 1.90	296.30 ± 3.81	29.50 ± 2.02	42.08 ± 1.83	32.34 ± 0.48
PEEK/GNP	338.8 ± 5.93	300.15 ± 2.61	30.12 ± 2.86	41.74 ± 0.34	33.14 ± 0.20
S-PEEK/GNP	341.5 ± 0.70	300.90 ± 0.14	30.00 ± 1.90	41.18 ± 2.66	31.11 ± 1.57

size–dependent structure associated with the parent PEEK and its synthesis route.

On the other hand, sulfonation reduces the degree of crystallinity by 1%. DSC is typically accurate to within a few percent[42] for these semi-crystalline polymers and so an ≈1% decrease in crystallinity is within the error of the technique. Thus, we conclude that CNS reinforcement increases the degree of crystallinity, while sulfonation has no significant effect on crystallinity of the printed PEEK and PEEK nanocomposites. This result suggests that the CNS incorporation achieved here both allows for FFF printing and does measurably alter the crystallinity of the printed parts from the baseline PEEK. The melting temperature increased by 1–2 °C with CNS reinforcement but decreased by ≈2 °C due to sulfonation. This slight decrease in the melting point due to sulfonation is attributed to the disruption on the chain backbone orientation preventing orientation and ordering of the crystallites formed, the crystalline unit cells, etc. As observed in SEM, the extent of pore formation on neat PEEK was less as compared to CNS-reinforced PEEK; therefore, the melting point remained unchanged. In addition to the thermophysical results from DSC, it is instructive to assess the surface topography of the printed structures, as obtained from SEM imaging of the surface of the scaffold samples, including with and without sulfonation (**Figure 4**). Minor differences are observed due to inclusion of the CNS, a similar finding to the DSC results. However, a clear difference between the sulfonated and nonsulfonated surfaces is noted. No pores are seen on the nonsulfonated samples (Figure 4a–c), whereas a porous network

was observed on the surfaces of sulfonated samples. As shown in Figure 4d–f, the extent of pore formation was more for nanocomposite (S-PEEK/CNT and S-PEEK/GNP) samples as compared to S-PEEK. The depth of the pores observed in all the sulfonated samples was of tens of micrometers (i.e., <1 print layer thickness of 100 µm). The sulfonation does not show any effect on the internal morphology of the 3D printed samples, which was confirmed from the SEM micrographs shown in Figure S2, Supporting Information. This observation confirms that the sulfonation process is a surface interaction controlled by the diffusion of H_2SO_4 and its reaction with the PEEK substrate; this indeed depends on PEEK's inherent properties, mostly determined through its synthesis route. Thus, the sulfonation recipe helped in creating pores as desired for enhanced bioactivity. The effect of the surface activation on the wetting angle is also shown in Figure 4, where representative contact angles from water droplet tests are plotted for each of the printed surfaces.

The hydrophilicity of the sample surfaces was analyzed using the sessile drop method by measuring the water contact angle (WCA),[35] as discussed in Section 2.4. Representative optical images of droplets for measurement of the WCA on all samples are shown in Figure 4. The results show a decrease in surface hydrophobicity due to CNS incorporation in PEEK. This is despite the usually assumed hydrophobicity of the CNS, which is explained by an increase in surface roughness caused by the CNS in the FFF AM, noted here and has been observed by others.[43,44] Sulfonation of 3D printed PEEK samples creates a porous 3D surface morphology due to the etching action of
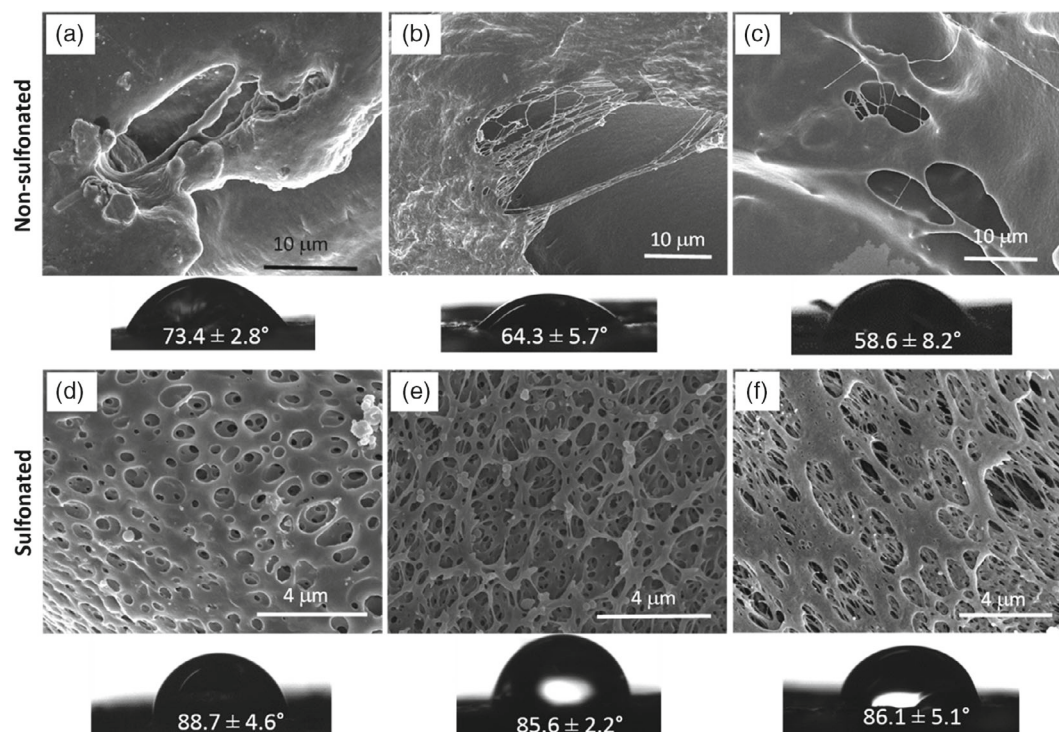
Figure 4. Representative SEM micrographs and wetting angles of the scaffold samples showing the effect of sulfonation on the surfaces for all sample types: a) PEEK, b) PEEK/CNT, c) PEEK/GNP, d) S-PEEK, e) S-PEEK/CNT, and f) S-PEEK/GNP.

concentrated sulfuric acid for the recipe used, leading to an inferred increase in the hydrophobicity of the samples via the contact angle method (compare Figure 4a,d). The sulfuric acid during sulfonation etches and creates a mesoporous surface architecture where water droplets, instead of penetrating into the pores,[33] sit on the morphology and yield a more hydrophobic surface than their nonsulfonated counterparts, even though CNS incorporation causes the PEEK surface to become more hydrophilic. We thus infer that for the sulfonated surfaces, the water droplet is not wetting the pores; that is, the water contact is non-Wenzel[45] (Cassie–Baxter).[46] To confirm the role of surface morphology, the possibility of any structural changes to the surface was assessed via XRD analysis, before and after sulfonation. No shift in peaks was observed through XRD analysis, indicating that only surface morphology affects the wettability. The results are shown in XRD spectra in Figure S3, Supporting Information. As can be seen from the photographs of the droplets, the increase in WCA for PEEK, Figure 4a ($\approx$73.4°) after sulfonation, and S-PEEK, Figure 4d ($\approx$88.7°), was less as compared to that observed for PEEK/CNT and PEEK/CNP nanocomposites. With sulfonation, the contact angle for PEEK/CNT and PEEK/GNP increased from $\approx$64.57° (PEEK/CNT, Figure 4b) to $\approx$85.6° (S-PEEK/CNT, Figure 4e) and $\approx$58.6° (PEEK/GNP, Figure 4c) to $\approx$86.1° (S-PEEK/GNP, Figure 4f). Other work has also shown that the sulfonation of PEEK at a small exposure time ($<$30 s) with sulfuric acid generally creates a hydrophilic surface, but a larger exposure time (30 s–5 min, as done here) creates a nanoporous surface where droplets suspend above the grooves and make it hydrophobic,[47] confirming the diffusion-controlled effect

of sulfonation. The apparent hydrophobicity increase with sulfonation does not lead to less, but rather more, bioactivity as shown later.

The representative thermographs obtained from DSC analysis are shown in Figure 3, in which the second heating (top) and cooling cycles (bottom) are shown as a function of temperature for both nonsulfonated and sulfonated samples. Thermal properties and degree of crystallization obtained from DSC analysis are shown in Table 2.

The thermograms clearly show that the breadth of the melting transition has changed for PEEK, including CNS/PEEK (see Figure 3 and S4, Supporting Information). This suggests that the nucleation process is altered, and that the size and perfection of crystals produced in all cases are not the same. Though the number of crystals is the same, the distribution of crystal sizes is not. Thus, the change in degree of crystallinity due to CNS incorporation and the manifested differences in size and perfection of crystals are expected to influence the macroscopic mechanical behavior. Indeed, any change in mechanical properties with the incorporation of CNS is due to the CNS mechanical reinforcement, degree of crystallinity changes induced by the CNS, change in crystal size distribution, and possibly surface changes due to sulfonation. The tensile properties of the 3D printed specimens were evaluated as discussed in Section 2 utilizing dogbone specimens (see Figure 1), and the effect of sulfonation was also assessed. Representative stress–strain curves of all sample types are shown in **Figure 5** and their corresponding tensile properties are reported in **Table 3**. The void fraction in the printed dogbones was not quantitatively assessed, but fracture
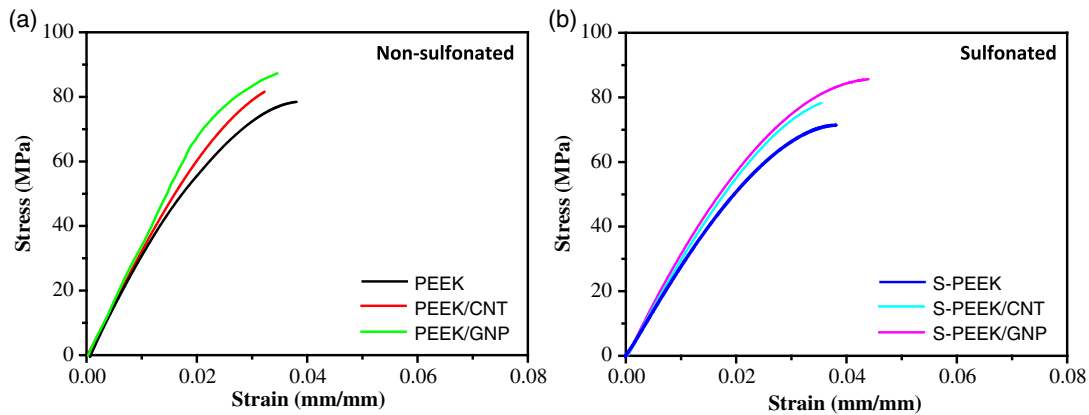
2000483 (6 of 11)

ADVANCED
SCIENCE NEWS
www.advancedsciencenews.com

ADVANCED
ENGINEERING
MATERIALS
www.aem-journal.com

Figure 5. Representative stress–strain curves of PEEK and PEEK nanocomposite samples, a) nonsulfonated and b) sulfonated PEEK.

Table 3. Tensile properties of the 3D-printed dogbone samples. Percentage changes in brackets refer to the PEEK baseline.

Samples	Modulus [GPa]	Yield strength [MPa]	Ultimate strength[a] [MPa]
PEEK	3.78 ± 0.05	77.69 ± 2.01	79.50 ± 1.93
S-PEEK	3.19 ± 0.02 (−15.60%)	71.18 ± 0.98 (−8.37%)	72.78 ± 1.75 (−8.45%)
PEEK/CNT	3.85 ± 0.12	82.69 ± 2.67 (+6.43%)	82.59 ± 2.67
S-PEEK/CNT	3.52 ± 0.23	76.88 ± 2.86	76.88 ± 2.86
PEEK/GNP	3.96 ± 0.09 (+4.75%)	85.47 ± 1.31 (+10.01%)	86.54 ± 1.60 (+8.85%)
S-PEEK/GNP	3.61 ± 0.08 (−4.76%)	83.41 ± 1.21 (+7.36%)	85.30 ± 0.36 (+7.29%)

[a]Provided for completeness; not valid according to the standard. Specimens failed both at the gage section and at the grip.

surface microscopy (optical and scanning electron) did not reveal significant levels of porosity, such as those that have been reported in other FFF structural polymers and composite printing.[48] With reference to PEEK as the baseline, sulfonation has the significant effect of reducing all measured mechanical properties significantly, on the order of 10–15%. All other trends are either not significant, or mixed, with reference to neat PEEK. CNT and GNP reinforcement increases properties relative to PEEK across all properties, but at a similar level to the sulfonation reductions, although GNP reinforcement has a significant positive effect on all three properties (5–10% increases only). Combined, the CNS reinforcement acts to enhance mechanical properties, while sulfonation reduces them, such that S-PEEK/CNT has the same properties as PEEK, while S-PEEK/GNP has a small (5%) decrease in modulus with ≈5% increases in strengths. Thus, the CNS reinforcement effect is to offset the sulfonation effects, effectively retaining the neat PEEK performance (or a little better). Typically, clear differences in mechanical behavior have been observed at higher levels of strain, above the ultimate tensile strength where PEEK resins with different synthesis routes show more or less ductile response.[21,49] At low strains, differences are minimal, as observed in this study. Moreover, bioactivity is not expected to influence the mechanical properties of implants in vivo. The mechanical response in a high-strain-regime (to analyze the effect of sulfonation and CNS) and long-term durability assessment of FFF AM–enabled PEEK nanocomposites is left to a subsequent study.

The fractured surfaces of the tensile test specimens were observed in SEM and the micrographs are shown in **Figure 6**. A low-magnification (≈100×) image of the surface shows the full fractured surface as print layers. Figure 6a–c are taken from the surface of nonsulfonated samples, whereas Figure 6d–f represent the surface of sulfonated samples. The dotted-line box in Figure 6 indicates the micrographs at the edge of the fractured surface. For sulfonated samples, the surface becomes more rough/porous relative to nonsulfonated samples. From Figure S2, Supporting Information, and Figure 6 it was confirmed that the effect of sulfonation was limited to the surface only.

3.2. Bioactivity

The printed cylindrical bioactivity scaffolds were utilized to assess apatite growth via immersion in SBF as evidenced by phase characterization (**Figure 7**a,b) and electron microscopy images (**Figure 8**). The peaks and intensities obtained from XRD were compared with the baseline PEEK without any apatite layer and the extra peaks at $2\theta° \approx 31.7°$ and $45.4°$ correspond to the presence of an apatite layer on the sample surface.[50] The intensities of these two apatite peaks were found to increase on the sulfonated samples (Figure 7b) as compared to non-sulfonated samples, consistent with the observation of greater apatite growth in the SEM. Note the mushroom-like[51] blooms of growth on the sulfonated samples versus the purely surface growth in the non-sulfonated series. Although the morphology
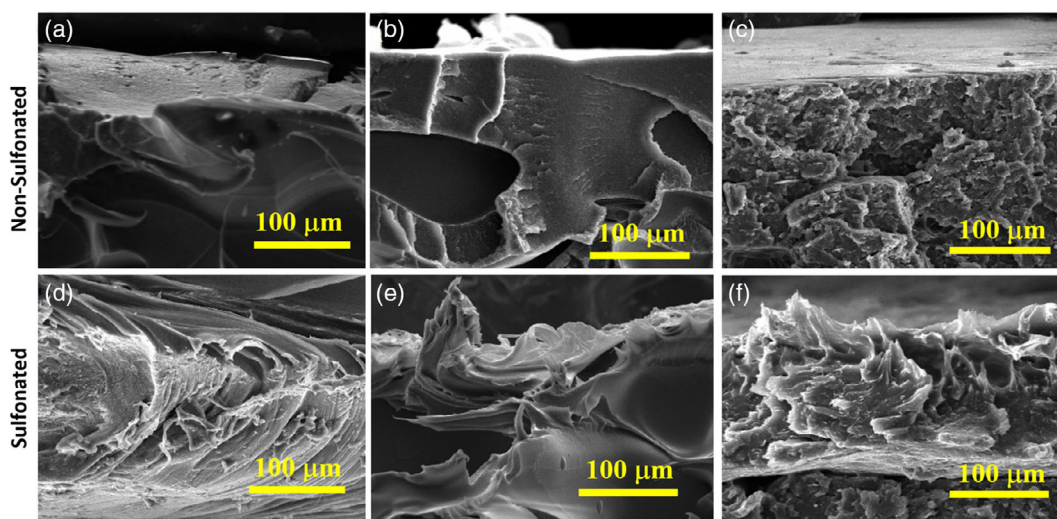
Figure 6. SEM images of failed dogbone specimens: a) PEEK, b) PEEK/CNT, c) PEEK/GNP, d) S-PEEK, e) S-PEEK/CNT, and f) S-PEEK/GNP.
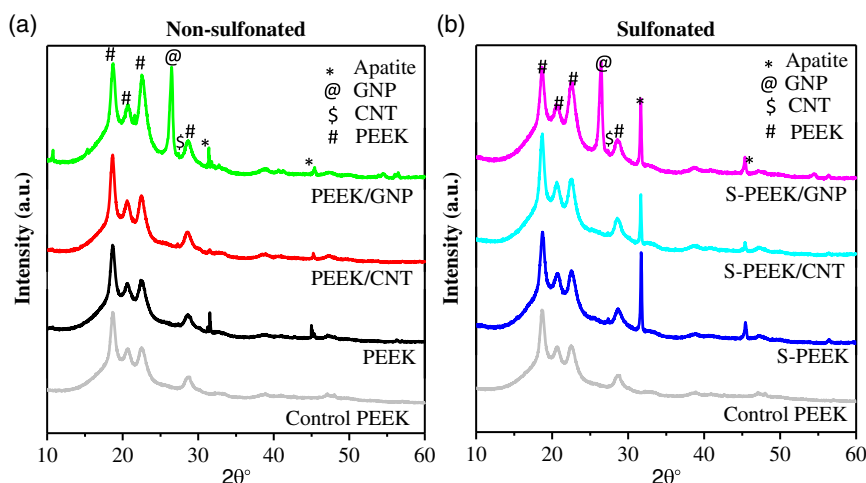

Figure 7. XRD spectra of apatite precipitation on the surface of PEEK and PEEK nanocomposite samples, a) nonsulfonated samples and b) sulfonated samples. "Control PEEK" refers to PEEK samples that have not undergone apatite growth.

is similar (porous structure), the degree of sulfonation obtained is not the same, leading to enhanced bioactivity of PEEK and its composites, as expected, despite the apparent hydrophobicity increase measured using the WCA test (as discussed previously). The differing degrees of sulfonation are interpreted as caused by the CNS and the inherent properties of each substrate.

The other representative peaks corresponding to PEEK, CNT, and GNP are labeled at their corresponding $2\theta°$ values. As the content of CNT was low (1 wt%), its representative peak ($\approx26.6°$) is not clearly observable in the XRD image of PEEK/CNT samples due to very low intensity as compared to PEEK. Energy-dispersive X-ray spectroscopy (EDS) with area mapping was applied to further substantiate the presence of apatite and very clear peaks of Ca (calcium) and P (phosphate) were observed for all the samples (Figure 8g–i). The other elements (Na, Mg, Cl, K, etc.) observed are from the SBF, which utilizes different salts of Na, Mg, and K.

For quantitative analysis of apatite growth, the fraction (%) of apatite grown was calculated from the area under the XRD peaks. The results are summarized in **Table 4**. Statistically significant differences are observed for sulfonated versus non-sulfonated samples, and for CNS versus sulfonated PEEK, indicating a synergistic effect of sulfonation and CNS toward bioactivity. The fraction of apatite growth due to sulfonation increased by $\approx3\%$ in PEEK, $\approx6\%$ in PEEK/CNT, and $\approx5\%$ in case of PEEK/GNP. The flower-like apatite morphology is observed after immersion tests in SBF (see in SEM micrograph in Figure 8a–c) and the surfaces were covered with a thin layer of apatite, whereas fully developed mushroom-like[51] apatite precipitation is observed after sulfonation (Figure 8d–f) and the surfaces of the samples were fully covered with a thicker layer of apatite. The increase in bioactivity of sulfonated samples can be explained by the electrostatic interaction of ions present in SBF with the functional group (SO_3H)
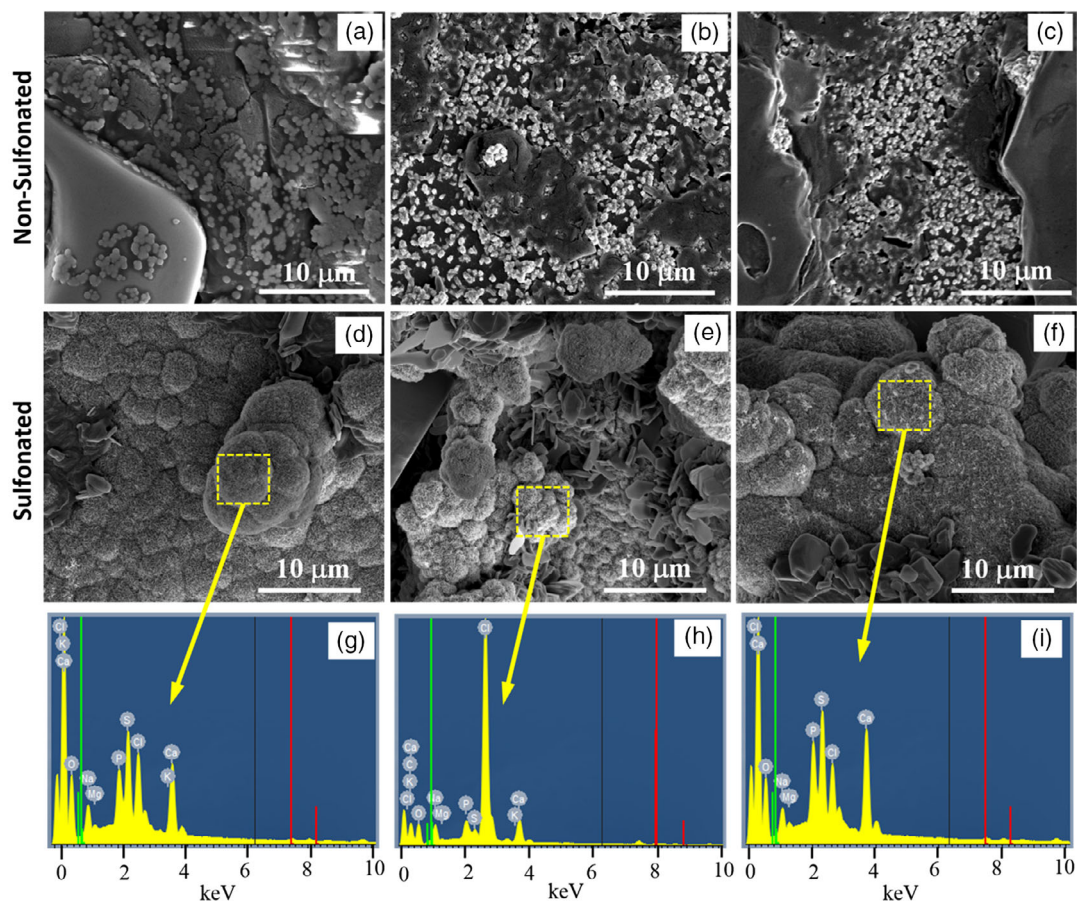
Figure 8. Bioactivity trends by observing apatite growth: SEM micrographs of the apatite precipitate on the surface of samples after 72 h of incubation for a) PEEK, b) PEEK/CNT, c) PEEK/GNP, d) S-PEEK, e) S-PEEK/CNT, and f) S-PEEK/GNP. g–i) The dotted yellow square in (d), (e), and (f), respectively, which highlights the region where area mapping was done to obtain EDS spectra from apatite layers grown on S-PEEK. S-PEEK/CNT, and S-PEEK/GNP.

Table 4. Quantification of apatite fraction grown on PEEK and PEEK nanocomposites from integrated intensity of XRD peaks. Percentage changes relative to PEEK are shown.

Samples	Fraction of apatite [%] (nonsulfonated samples)	Fraction of apatite [%] (sulfonated samples)
PEEK	7.96 ± 0.23	10.89 ± 0.17 (+36.80%)
PEEK/CNT	6.48 ± 1.01 (−18.59%)	12.50 ± 0.71 (+57.03%)
PEEK/GNP	8.52 ± 1.30	14.05 ± 0.80 (+76.50%)

produced by sulfonation.[20] The SO_3H present on the surface of sulfonated samples dissociates into ions (SO_3^- and H^+) in SBF, forming a negatively charged surface. However, the positively charged calcium ions (Ca^{2+}) present in SBF cover the substrate, creating a positively charged surface. The negatively charged phosphate ions (HPO_4^{2-}) in SBF are attracted by the positively charged surface, leading to the formation of a calcium hydrogen phosphate (apatite) layer by consuming HPO_4^{2-}, Ca^{2+}, and OH^- from SBF.[52] Detailed characterization with a particular emphasis on biocompatibility and cytotoxicity responses with mammalian cells of our AM-enabled PEEK nanocomposites will be explored in a subsequent study.

4. Conclusion

In this study, we developed CNS-reinforced PEEK filament feedstocks (CNT/PEEK and GNP/PEEK) via melt extrusion for FFF AM toward biomedical structural applications where the mechanical response of interest is in the low-strain linear-elastic regime. Subsequently, in vitro bioactivity and mechanical characteristics of 3D printed PEEK and PEEK polymer nanocomposite scaffolds and dogbone test specimens were analyzed with and without sulfonation. CNS reinforcement increased the degree of crystallinity, while sulfonation has no significant effect on crystallinity of the printed PEEK and PEEK nanocomposites, although further analysis of changes to crystallite size and distribution would be needed to address effects that typically manifest in the higher-strain hysteretic regime of the mechanical response. Sulfonation with an exposure time of 5 min creates a mesoporous 3D surface architecture due to the etching action of concentrated sulfuric acid. While sulfonation should aid bioactivity by increasing the hydrophilicity of the surface, WCA tests reveal the opposite trend. Water droplets used to infer surface energy, instead of penetrating into the pores, sit on the morphology and yield a droplet test that implies a more hydrophobic surface than the non-sulfonated counterparts (increase in WCA

of S-PEEK by ≈15°, S- PEEK/CNT composites by ≈20°, and S-PEEK/GNP composites by 27°). We conclude that the surface is more hydrophilic, but the WCA test gives a net hydrophobic WCA. Subsequent SBF bioactivity tests reveal a synergy between the CNS and the sulfonation, exhibiting apatite growth on the sample surfaces. The electrostatic interaction of ions present in SBF with the functional group (SO_3H) produced by sulfonation enhances the bioactivity by ≈36% for S-PEEK, ≈57% for S-PEEK/CNT, and ≈77% for S-PEEK/GNP. A fully grown mushroom-like apatite precipitation is observed after sulfonation for the CNS-reinforced PEEK. The differing degree of sulfonation caused by the combined effect of CNS and the inherent properties of the substrate, as well as the creation of biofunctional groups during SBF tests would help to improve the osseointegration of the bone implants. Furthermore, the CNS reinforcement acts to enhance mechanical properties in the low-strain regime, while sulfonation reduces, such that S-PEEK/CNT has effectively the same properties as PEEK; for example, S-PEEK/GNP has a small (5%) decrease in modulus with ≈5% increases in strengths. The study of effect of sulfonation and CNS on the mechanical response in a high-strain-regime and additional work to understand the manifestation of differences in size and perfection of crystals, which might more significantly affect hysteretic processes, are left to a subsequent study. Detailed characterization with a particular emphasis on biocompatibility and cytotoxicity responses with mammalian cells as well as long-term durability assessment of our AM-enabled PEEK nanocomposites would be needed to validate the true potential for in vivo use of these novel composites. AM of PEEK with CNS reinforcement opens up many opportunities for structural and functional applications, including self-sensing scaffolds in orthopedics. Further work to optimize processing parameters, including printing parameters, and sulfonation times, should lead to additively manufactured PEEK with CNS reinforcement that has enhanced bioactivity and additional functionality beyond structural properties.

Supporting Information

Supporting Information is available from the Wiley Online Library or from the author.

Acknowledgements

Conflict of Interest

The authors declare no conflict of interest.

Keywords

additive manufacturing, bioactivity, carbon nanotube/polyetheretherketone (CNT/PEEK) and graphene nanoplatelet (GNP/PEEK) nanocomposites, fused filament fabrication, sulfonation

[1] a) J. I. Kroschwitz, *Concise Encyclopedia of Polymer Science and Engineering*, Wiley, New York **1990**; b) J. M. Toth, M. Wang, B. T. Estes, J. L. Scifert, H. B. Seim III, A. S. Turner, *Biomaterials* **2006**, *27*, 324.

[2] S. M. Kurtz, J. N. Devine, *Biomaterials* **2007**, *28*, 4845.

[3] a) I. V. Panayotov, V. Orti, F. Cuisinier, J. Yachouh, *J. Mater. Sci.: Mater. Med.* **2016**, *27*, 118; b) M. Jarman-Smith, *Med. Device Technol.* **2008**, *19*, 12.

[4] S. M. Kurtz, *PEEK Biomaterials Handbook*, William Andrew Publishing, Norwich, United States **2019**, p. 11.

[5] R. J. Morrison, S. J. Hollister, M. F. Niedner, M. G. Mahani, A. H. Park, D. K. Mehta, R. G. Ohye, G. E. Green, *Sci. Transl. Med.* **2015**, *7*, 285ra64.

[6] S. V. Murphy, A. Atala, *Nat. Biotechnol.* **2014**, *32*, 773.

[7] S. Kumar, B. L. Wardle, M. F. Arif, J. Ubaid, *Adv. Eng. Mater.* **2018**, *20*, 1700883.

[8] M. Schmidt, D. Pohle, T. Rechtenwald, *CIRP Ann.* **2007**, *56*, 205.

[9] a) R. Singh, R. Sharma, N. Ranjan, in *Reference Module in Materials Science and Materials Engineering* (Ed: J. G. R. Sereni), Elsevier, Oxford **2017**, pp. 1–28; b) O. A. Mohamed, S. H. Masood, J. L. Bhowmik, in *Reference Module in Materials Science and Materials Engineering* (Ed: S. Hashmi), Elsevier **2016**, https://doi.org/10.1016/B978-0-12-803581-8.04026-1; c) K. Boparai, R. Singh, in *Reference Module in Materials Science and Materials Engineering*, Elsevier **2017**, https://doi.org/10.1016/B978-0-12-803581-8.04166-7; d) J. Walker, M. Santoro, *Bioresorbable Polymers for Biomedical Applications*, Elsevier **2017**, p. 181; e) S. Singh, R. Singh, in *Reference Module in Materials Science and Materials Engineering* (Ed: S. Hashmi), Elsevier **2017**, https://doi.org/10.1016/B978-0-12-803581-8.10349-2; f) M. Garcia-Leiner, O. Ghita, R. McKay, S. M. Kurtz, *PEEK Biomaterials Handbook*, Elsevier **2019**, p. 89.

[10] a) S. Berretta, R. Davies, Y. T. Shyng, Y. Wang, O. Ghita, *Polym. Testing* **2017**, *63*, 251; b) R. Davies, Y. Wang, O. Ghita, in *20th Int. Conf. on Composite Materials Copenhagen* 2015, http://www.iccm-central.org/Proceedings/ICCM20proceedings/papers/paper-3401-3.pdf; c) J. Gonçalves, P. Lima, B. Krause, P. Pötschke, U. Lafont, J. R. Gomes, C. S. Abreu, M. C. Paiva, J. A. Covas, *Polymers* **2018**, *10*, 925.

[11] a) J. Ubaid, B. L. Wardle, S. Kumar, *Sci. Rep.* **2018**, *8*, 13592; b) J. Liljenhjerte, P. Upadhyaya, S. Kumar, *Addit. Manuf.* **2016**, *11*, 40; c) S. Kumar, B. L. Wardle, M. F. Arif, *ACS Appl. Mater. Interfaces* **2016**, *9*, 884.

[12] a) K. Upadhyay, R. Dwivedi, A. K. Singh, *Advances in 3D Printing & Additive Manufacturing Technologies*, Springer, Singapore **2017**, p. 9; b) M. Montero, S. Roundy, D. Odell, S.-H. Ahn, P. K. Wright, *Soc. Manuf. Eng.* **2001**, *10*; c) S.-H. Ahn, M. Montero, D. Odell, S. Roundy, P. K. Wright, *Rapid Prototyping J.* **2002**, *8*, 248.

[13] Y. Li, S. Gao, R. Dong, X. Ding, X. Duan, *J. Mater. Eng. Perform.* **2018**, *27*, 492.

[14] H. Wu, A. Kafi, H. Kim, R. Shah, S. Bateman, J. Koo, *Additive Manufacturing of Flame-retardant Polyamide 6 Nanocomposites Via Fused Filament Fabrication (FFF)*, Sampe, North America **2019**.

[15] a) Y.-G. Zhou, B. Su, L.-s. Turng, *Rapid Prototyping J.* **2017**, *23*, 869; b) O. S. Carneiro, A. F. Silva, R. Gomes, *Mater. Design* **2015**, *83*, 768.

[16] W. C. Smith, R. W. Dean, *Polymer Test.* **2013**, *32*, 1306.

[17] K. Gnanasekaran, T. Heijmans, S. Van Bennekom, H. Woldhuis, S. Wijnia, G. de With, H. Friedrich, *Appl. Mater. Today* **2017**, *9*, 21.

[18] a) M. F. Arif, S. Kumar, K. M. Varadarajan, W. J. Cantwell, *Mater. Design* **2018**, *146*, 249; b) B. Chen, S. Berretta, K. Evans, K. Smith, O. Ghita, *Appl. Surface Sci.* **2018**, *428*, 1018; c) S. Xiaoyong, C. Liangcheng, M. Honglin, G. Peng, B. Zhanwei, L. Cheng, in *9th Int. Conf. on Measuring Technology and Mechatronics Automation*, IEEE, Changsha, China **2017**; d) F. S. Senatov, A. V. Chubrik, A. V. Maksimkin, E. A. Kolesnikov, A. I. Salimon, *Mater. Lett.* **2019**, *239*, 63; e) D. Briem, S. Strametz, K. Schröoder, N. Meenen, W. Lehmann, W. Linhart, A. Ohl, J. Rueger, *J. Mater. Sci. Mater. Med.* **2005**, *16*, 671; f) R. Kumar, M. Mamlouk, K. Scott, *RSC Adv.* **2014**, *4*, 617.

[19] a) S. K. Reddy, S. Kumar, K. M. Varadarajan, P. R. Marpu, T. K. Gupta, M. Choosri, *Mater. Sci. Eng.: C* **2018**, *92*, 957; b) M. F. Arif, S. Kumar, T. K. Gupta, K. M. Varadarajan, *Compos. A: Appl. Sci. Manuf.* **2018**, *113*, 141.

[20] Y. Zhao, H. M. Wong, W. Wang, P. Li, Z. Xu, E. Y. W. Chong, C. H. Yan, K. W. K. Yeung, P. K. Chu, *Biomaterials* **2013**, *34*, 9264.

[21] M. Garcia-Leiner, M. T. Reitman, M. J. El-Hibri, R. K. Roeder, *Polym. Eng. Sci.* **2017**, *57*, 955.

[22] M. Arif, H. Alhashmi, K. Varadarajan, J. H. Koo, A. Hart, S. Kumar, *Compos. B: Eng.* **2020**, *184*, 107625.

[23] T. Kokubo, H. Kushitani, S. Sakka, T. Kitsugi, T. Yamamuro, *J. Biomed. Mater. Res.* **1990**, *24*, 721.

[24] a) M. Saini, Y. Singh, P. Arora, V. Arora, K. Jain, *World J. Clin. Cases* **2015**, *3*, 52; b) R. Agarwal, A. J. García, *Adv. Drug Deliv. Rev.* **2015**, *94*, 53.

[25] a) A. J. Kassick, S. S. Yerneni, E. Gottlieb, F. Cartieri, Y. Peng, G. Mao, A. Kharlamov, M. C. Miller, C. Xu, M. Oh, T. Kowalewski, B. Cheng, P. G. Campbell, S. Averick, *ACS Appl. Bio Mater.* **2018**, *1*, 1047; b) N. T. Evans, F. B. Torstrick, C. S. D. Lee, K. M. Dupont, D. L. Safranski, W. A. Chang, A. E. Macedo, A. S. P. Lin, J. M. Boothby, D. C. Whittingslow, R. A. Carson, R. E. Guldberg, K. Gall, *Acta Biomater.* **2015**, *13*, 159; c) B. Yuan, Q. Cheng, R. Zhao, X. Zhu, X. Yang, X. Yang, K. Zhang, Y. Song, X. Zhang, *Biomaterials* **2018**, *170*, 116.

[26] a) A. Iulianelli, G. Clarizia, A. Gugliuzza, A. Ebrasu, A. Bevilacqua, F. Trotta, A. Basile, *Int. J. Hydrogen Energy* **2010**, *35*, 12688; b) A. M. Martos, M. Biasizzo, F. Trotta, C. del Río, A. Várez, B. Levenfeld, *Eur. Polym. J.* **2017**, *93*, 390; c) V. S. Rangasamy, S. Thayumanasundaram, N. De Greef, J. W. Seo, J. P. Locquet, *Eur. J. Inorg. Chem.* **2015**, *2015*, 1282.

[27] a) J. Zhao, L. Guo, J. Wang, *J. Membr. Sci.* **2018**, *563*, 957; b) W. Xu, X. Li, J. Cao, H. Zhang, H. Zhang, *Sci. Rep.* **2014**, *4*, 4016; c) G. Sivasubramanian, K. Hariharasubramanian, P. Deivanayagam, J. Ramaswamy, *Polym. J.* **2017**, *49*, 703.

[28] R. Brum, P. Monich, M. Fredel, G. Contri, S. Ramoa, R. Magini, C. Benfatti, *J. Mater. Sci.: Mater. Med.* **2018**, *29*, 132.

[29] a) J. N. Coleman, U. Khan, W. J. Blau, Y. K. Gun'ko, *Carbon* **2006**, *44*, 1624; b) P.-C. Ma, N. A. Siddiqui, G. Marom, J.-K. Kim, *Compos. A: Appl. Sci. Manuf.* **2010**, *41*, 1345; c) G. Mittal, V. Dhand, K. Y. Rhee, S.-J. Park, W. R. Lee, *J. Ind. Eng. Chem.* **2015**, *21*, 11; d) Z. Spitalsky, D. Tasis, K. Papagelis, C. Galiotis, *Prog. Polym. Sci.* **2010**, *35*, 357.

[30] P. Verma, V. Choudhary, *J. Appl. Polym. Sci.* **2015**, *132*, 41734.

[31] S. Reddy, S. Kumar, K. Varadarajan, P. Marpu, T. K. Gupta, M. Choosri, *Mater. Sci. Eng.: C* **2018**, *92*, 957.

[32] O. B. Blundell, B. N. Osborn, *Ploymer* **1983**, *24*, 953.

[33] W. Wang, C. J. Luo, J. Huang, M. Edirisinghe, *J. R. Soc. Interface* **2019**, *16*, 20180955.

[34] K. Anselme, *Biomaterials* **2000**, *21*, 667.

[35] A. Calvimontes, Preprint **2018**, 10.20944/preprints201802.0018.v1.

[36] a) J. M. Chacón, M. A. Caminero, E. García-Plaza, P. J. Núñez, *Mater. Design* **2017**, *124*, 143; b) J. J. Laureto, J. M. Pearce, *Polym. Test.* **2018**, *68*, 294.

[37] S. Kotani, T. Yamamuro, *J. Biomed. Mater. Res.* **1991**, *25*, 1363.

[38] a) T. Kokubo, H. Takadama, *Biomaterials* **2006**, *27*, 2907; b) A. A. Zadpoor, *Mater. Sci. Eng.: C* **2014**, *35*, 134.

[39] E. Kalantari, S. M. Naghib, *Mater. Sci. Eng.: C* **2019**, *98*, 1087.

[40] A. K. Patel, K. Balani, *Mater. Sci. Eng.: C* **2015**, *46*, 504.

[41] a) M. A. Kazakova, A. G. Selyutin, N. V. Semikolenova, A. V. Ishchenko, S. I. Moseenkov, M. A. Matsko, V. A. Zakharov, V. L. Kuznetsov, *Compos. Sci. Technol.* **2018**, *167*, 148; b) B. Yang, D. Wang, F. Chen, L.-F. Su, J.-B. Miao, P. Chen, J.-S. Qian, R. Xia, J.-W. Liu, *J. Macromol. Sci. B* **2019**, *58*, 290.

[42] a) Y. Kong, J. N. Hay, *Polymer* **2002**, *43*, 3873; b) A. P. Gray, *Thermochim. Acta* **1970**, *1*, 563.

[43] K. Gnanasekaran, T. Heijmans, S. van Bennekom, H. Woldhuis, S. Wijnia, G. de With, H. Friedrich, *Appl. Mater. Today* **2017**, *9*, 21.

[44] X. Wei, D. Li, W. Jiang, Z. Gu, X. Wang, Z. Zhang, Z. Sun, *Sci. Rep.* **2015**, *5*, 11181.

[45] R. N. Wenzel, *Ind. Eng. Chem.* **1936**, *28*, 988.

[46] A. B. D. Cassie, S. Baxter, *Trans. Faraday Soc.* **1944**, *40*, 546.

[47] X.-M. Li, D. Reinhoudt, M. Crego-Calama, *Chem. Soc. Rev.* **2007**, *36*, 1350.

[48] E. Dugbenoo, M. F. Arif, B. L. Wardle, S. Kumar, *Adv. Eng. Mater.* **2018**, *20*, 1800691.

[49] a) R. Chivers, D. Moore, *Polymer* **1994**, *35*, 110; b) J.-N. Chu, J. M. Schultz, *J. Mater. Sci.* **1990**, *25*, 3746; c) M. Yuan, J. A. Galloway, R. J. Hoffman, S. Bhatt, *Polym. Eng. Sci.* **2011**, *51*, 94.

[50] F. Alam, A. Kumar, A. K. Patel, R. K. Sharma, K. Balani, *JOM* **2015**, *67*, 688.

[51] J. Kunze, L. Müller, J. M. Macak, P. Greil, P. Schmuki, F. A. Müller, *Electrochim. Acta* **2008**, *53*, 6995.

[52] H.-M. Kim, T. Himeno, M. Kawashita, T. Kokubo, T. Nakamura, *J. R. Soc. Interface* **2004**, *1*, 17.

2000483 (11 of 11)